Noble gas 'snapshot' of the continental lithospheric mantle from CO_2 well gases.

Stuart M.V. Gilfillan* and Chris J. Ballentine

School of Earth, Atmospheric and Environmental Sciences (SEAES),
The University of Manchester,
Oxford Road,
Manchester.
M13 9PL
United Kingdom

*Author to whom correspondence should be addressed, now at;

School of Geosciences, University of Edinburgh, Grant Institute, Kings Buildings,

West Mains Road, Edinburgh, U.K. EH9 3JW

E-mail: stuart.gilfillan@ed.ac.uk

Telephone: +44 (0) 131 650 7010

Fax: +44 (0) 131 668 3184

1. INTRODUCTION

The subcontinental lithospheric mantle (SCLM) constitutes a significant portion of the upper mantle and sources magmatic volatiles to the continents above, yet its geochemical signature and evolution remain poorly constrained. Traditionally, upper mantle characteristics have been deduced from the more conveniently sampled convective mantle, via mid-ocean ridge and ocean island volcanics. The SCLM is a reservoir isolated from this convective portion of the upper mantle and has developed its own unique isotopic, major and trace element signature. It is also possible that the SCLM contains a significant quantity of noble gases and other trace elements and that re-entrainment of this material into the deeper mantle may contribute to the characteristic mantle signature sampled at ocean islands [1].

Noble gases, and the $^{3}He/^{4}He$ ratio in particular, provide vital information about the character and processes controlling the mantle volatile source. Previous studies have identified that the isotopic ratio of helium within the SCLM is more radiogenic than that of the mid ocean ridge (MORB) source mantle [2-4]. Recent work by Day et al. (2005) reported $^{3}He/^{4}He$ ratios that are more radiogenic than MORB from continental intra-plate alkaline volcanics from Canada, South Africa and Uganda, corroborating these earlier studies. The origin of this radiogenic He is enigmatic and several explanations have been proposed including; alteration of the MORB source mantle by either addition of sediments [3] or isolation and ageing [5], regional low $^{3}He/^{4}He$ plume sources [6, 7]. The neon and argon isotopic composition of the SCLM is even less well constrained, with previous studies documenting small anomalies compared to air values [8, 9]. These

observations have been explained by atmospheric contamination or the recycling of an atmospheric component back into the lithospheric mantle. Recently, Matsumoto et al. (2001) have proposed that atmospheric noble gases can be recycled into the lithospheric mantle and that the SCLM can potentially store these atmospheric noble gases. This issue is critical to rare gas budgets as the SCLM can be delaminated and recycled back into the convecting mantle [10].

Our current knowledge of the characteristics of the SCLM has been deduced from magmas derived from melting of this portion of the mantle and from xenoliths trapped by rapidly rising magmas. However, typically magmas that reach the surface subaerially are strongly degassed and apart from occasional phenocrysts, do not contain a significant quantity of noble gases [4, 11]. Hence the vast majority of data regarding the SCLM has been obtained from analysis of ultramafic xenoliths sourced from continental volcanic provinces. Unfortunately, whilst some volcanic localities allow local mantle $^{3}He/^{4}He$ ratio to be determined from these xenoliths, suitable samples are not always available, and air contamination of this sample type precludes resolution of the heavy mantle-derived noble gases.

Magmatic CO_2 well gases provide a new and exciting resource that enables the $^{3}He/^{4}He$, heavy noble gas isotope and relative abundance determination of the mantle source [12, 13]. Primordial noble gas isotopes have been studied in well gases since 1961 [14-21], but until recently their use in investigating the SCLM in detail has been limited. We present here noble gas analyses from magmatic

CO_2 well gases in the SW US which provide a unique insight into the volatile character of the SCLM sourcing the Cenozoic volcanism in the region. We have been able to resolve the mantle He, Ne and Ar ratios of the mantle source beneath two natural magmatic CO_2 reservoirs. Our new data from the Sheep Mountain field suggests that that the process responsible for reducing the $^3He/^4He_{mantle}$ ratio within the SCLM is radiogenic production within the mantle which allows us to explore models proposed to account for the SCLM evolution and volatile origin in greater detail than has been previously possible.

2. TECTONIC SETTING OF THE COLORADO PLATEAU AND ROCKY MOUNTAIN NATURAL CO_2 RESERVOIRS

The Colorado Plateau is a massive, high-standing tectonic block located in the south-western US, centred on the Four Corners of the states of Colorado, New Mexico, Utah, and Arizona (Fig. 1). It is abruptly flanked to the east by the majestic Rocky Mountains, the result of at least 2 km of uplift during the Laramide Orogeny and later Cenozoic uplifts [22].

2.1. Cenozoic Volcanism and the Colorado Plateau Uplift Event

In the late Cenozoic the cessation of subduction along the Pacific margin triggered extensive basic magmatic activity and accompanying lithosphere extension, block faulting and local uplift across the western United States [23]. These events had a dramatic effect on the Colorado Plateau which was uplifted some 2 km, with the most recent uplift event raising the south-western margin of the Plateau by approximately 1 km between 6 and 1 Ma [22]. However, it is the lack of significant deformation of the region which is even more significant, especially given the rapid nature of the uplift event. Both the Rio Grande rift and the Basin and Range province have experienced similar degrees of uplift and have suffered extensive compression and internal faulting, whilst the Colorado Plateau has remained a rigid block, resisting significant deformation [22].

The scale of the uplift event and the dominance of basaltic magmatism throughout implies some degree of mantle influence in the process, though the exact mechanism is still highly contentious. Several mechanisms have been proposed including crustal thickening caused by horizontal compression [24];

thermal expansion due to a mantle plume [23, 25]; a reduction in the density of the mantle caused by physical thinning or thermal expansion of the lithosphere lid or by the presence of a plume component [22] and complete or partial lithosphere delamination [26-28].

2.2. Tectonic Setting of Colorado Plateau and Rocky Mountain CO_2 Reservoirs

Within the Colorado Plateau and surrounding Rocky Mountain region there are at least nine producing or abandoned gas fields that contain up to 2800 billion m^3 of natural CO_2 [29]. In this paper we detail the results from two separate gas fields, namely Sheep Mountain, (Huerfano County, CO) and Bravo Dome, (Harding County, NM), both of which contain extremely high concentrations of magmatic CO_2 (Fig. 4.1.). The background geology of these sites is covered in detail in Gilfillan et al., 2006.

2.2.1. Sheep Mountain

The Sheep Mountain gas field is located at the northern end of the Raton Basin, some 45 km northwest of the town of Walsenberg, south central Colorado (Fig 4.1.). This region was extensively tilted and folded as a result of uplift to the west during by the Laramide Orogeny in the late Cretaceous-early Tertiary time. [30]. As a result of this event, large volumes of lava were extruded from vents along the Sierra Grande arch, within the Raton Basin and on the eastern margin of the basin. Intrusive activity accompanied these volcanics, producing extensive sills and laccoliths including the distinctive peaks of Little Sheep Mountain, Sheep Mountain and Dike Mountain. The nearest intrusive to the field is the Sheep

Mountain – Little Sheep Mountain laccolith, which consists of intermediate-acidic igneous rocks and trends north-northwest covering an area of approximately 13 km^2 [30-32].

2.2.2. Bravo Dome

The Bravo Dome field (originally named the Bueyeros field) is located south of Cortez in Harding County, northeastern New Mexico (Fig. 2). It is a large field (2000 km^2) which consists of a northwest trending anticlinal nose situated on the spur of the Sierra Grande arch [33]. The field is bounded by the Tucumari basin to the south and the Dalhart Basin to the north [34, 35]. CO_2 from the field has been studied since the 1960s. [14, 15, 17, 21]. Phinney (1978) reported the first ^3He excess in the gas, which they attributed to a primordial mantle source. This was confirmed by Staudacher (1987) who showed that the noble gas pattern from CO_2 within the field was indistinguishable from that of fresh MORB glasses and this has been reinforced by the two recent studies of Caffee et al., (1999) and Ballentine et al. (2005). CO_2 is believed to have migrated from vents associated with the nearby Rio Grande rift volcanic activity, via deep seated faults that cut through the fractured basement below the reservoir [33]. Known volcanic activity in the region dates from 100,000 to 8,000 years ago suggesting that the field filled recently [36].

3. SAMPLE COLLECTION AND ANALYTICAL TECHNIQUES

Samples from the gas fields were collected directly from producing wellheads that tap the natural gas reservoirs. Sample localities were chosen on site to provide a wide range of depth and spatial distribution across the fields. Samples were collected via the conventional ¾-inch National Pipe Thread (NPT) sample port of the well head using 'Swagelok©' 300 ml stainless steel sampling cylinders sealed at both ends with high-pressure valves. This technique is outlined in detail in Gilfillan et al., (2006a).

^{4}He, ^{20}Ne, ^{40}Ar, ^{84}Kr, ^{132}Xe, $^{3}He/^{4}He$, $^{20}Ne/^{22}Ne$, $^{21}Ne/^{22}Ne$, $^{40}Ar/^{36}Ar$ and $^{130}Xe/^{136}Xe$ for Sheep Mountain were determined at the University of Manchester using an all metal purification line and a MAP 215 mass spectrometer using the procedures outlined in Gilfilan et al., (2006). Blank levels were negligible compared to original sample size for all isotopes except ^{20}Ne, which was typically <1%. The Bravo Dome samples documented in this study were analyzed at ETH (Eidgenössische Technische Hochschule; Federal Institute of Technology), and are published in Ballentine et al. (2005).

4. RESULTS

A total of 32 deep CO_2 well gas samples from the two gas fields were analyzed as part of a comprehensive study of CO_2 reservoirs and natural seeps in the Colorado Plateau and Rocky Mountain regions. Table 1. documents the sample location, producing formation and noble gas isotopic composition; $^{3}He/^{4}He$, $^{20}Ne/^{22}Ne$, $^{21}Ne/^{22}Ne$, $^{40}Ar/^{36}Ar$ and $^{130}Xe/^{136}Xe$. Table 2. outlines the noble gas abundance measurements; ^{4}He, ^{20}Ne, ^{40}Ar, ^{84}Kr and ^{130}Xe and was also determined. Recent sample collection and analysis at Manchester by Holland and Ballentine (2006) has expanded the mantle rich portion of the Bravo Dome dataset. However, we use the earlier values determined at ETH by Ballentine (2005) which have greater crustal contributions, and therefore provide a clearer resolution of the crustal end member in the field.

4.1. Helium

$^{3}He/^{4}He$ values from the Bravo Dome field exhibit a coherent variation from 0.764 to 4.07 Ra on moving eastwards within the field (Fig. 2.) (4.26 Ra has been measured in a previous study). This corresponds with a significant increase in both ^{3}He and ^{4}He concentrations (Fig. 3.) and highlights that the high mantle $^{3}He/^{4}He$ input value is being reduced by the addition of crustal radiogenic ^{4}He. This is a stark contrast to the $^{3}He/^{4}He$ values from the Sheep Mountain field which are remarkably uniform and predominantly lower, varying from 0.916 up to 1.06 Ra (Fig. 3). No spatial control on this variation exists indicating that the field has either been homogenized over time or that crustal radiogenic ^{4}He and mantle derived ^{3}He were well mixed prior to input into the gas field.

Absolute ^{3}He concentrations in both fields are high, ranging from 4.96 to 9.84 x 10^{-10} $cm^3STP(^3He)/cm^3$ within Sheep Mountain and 2.10 to 4.34 x 10^{-10} $cm^3STP(^3He)/cm^3$ which plot directly within the pure magmatic CO_2 range of 1 x 10^{-10} and 5 x 10^{-10} $cm^3STP(^3He)/cm^3$ [37, 38]. Measured $CO_2/^3He$ ratios from both fields plot within the magmatic range of 1 x 10^9 – 1 x 10^{10} confirming that the CO_2 in the fields has a predominantly mantle origin (Gilfillan et al., 2006).

4.2. Neon

Within the Bravo Dome field both the variation in $^{20}Ne/^{22}Ne$ from 9.93 ± 0.09 to 11.88 ± 0.05 and $^{21}Ne/^{22}Ne$ values from 0.0501 ± 0.0003 to 0.0579 ± 0.0005 exhibit a similar spatial correlation as that observed in the $^3He/^4He$ values (Fig. 3.). Neon isotopes measurements from Sheep Mountain exhibit a significantly larger variation than that observed in the $^3He/^4He$ ratios (Fig. 3.). $^{20}Ne/^{22}Ne$ values measured in field vary between 9.84 ± 0.03 and 10.29 ± 0.08. $^{21}Ne/^{22}Ne$ varies between 0.031 ± 0.0003 and 0.614 ± 0.0003, exhibiting a clear mixing relationship with the air sourced from the groundwater, indicated by a reduction of the ratio corresponding to an increase of air-derived ^{20}Ne concentrations (Fig. 5.(a)).

As Ne is derived from three isotopically distinct sources, (namely the crust, mantle and air), the contribution of each of these sources to any sample can be resolved using the technique outlined by Ballentine (1997). This is because any sample that contains a mix of these components must plot within the envelope defined by the well known $^{20}Ne/^{22}Ne$ and $^{21}Ne/^{22}Ne$ air and crust end members

and the resolved mantle end member values of 12.5 for $^{20}Ne/^{22}Ne$ and 0.06 for $^{21}Ne/^{22}Ne$ [12].

Fig. 4. highlights the distinct crust/mantle/air mixing trends that can be observed in the two fields. Sheep Mountain exhibits a clear mixing trend between air and a pre-mixed crust and mantle component. Bravo Dome, on the other hand, highlights mixing between an original mantle component and an air/crust mixture. This most probably reflects interaction of the Sheep Mountain well gases with a young groundwater which contains negligible crustal noble gases, compared to the older groundwater containing accumulated radiogenic noble gases which has interacted with the Bravo Dome reservoir. Alternatively, this could also reflect differing degrees of radiogenic production within the mantle sourcing the well gases. Distinction between these two theories is discussed in more detail in section 4.6.1.

4.3. Argon

Bravo Dome $^{40}Ar/^{36}Ar$ ratios vary from 2,800 up to 22,550 and also exhibit the same coherent spatial variation as observed in both the $^{3}He/^{4}He$ and the $^{20}Ne/^{22}Ne$. $^{40}Ar/^{36}Ar$ ratios in the Sheep Mountain field vary from 4,400 to 21,200. A lowering of the $^{40}Ar/^{36}Ar$ ratio corresponding to increasing ^{36}Ar concentrations highlights mixing of air, derived from the ASW, with the gas within the reservoir (Fig. 5(b)). This is similar to the relationship observed in the Ne dataset.

Atmospheric contributions to ^{40}Ar can be corrected for using the formula outlined by Ballentine et al., (2002);

$$\left[{}^{40}Ar\right]_{corrected} = \left[{}^{40}Ar\right]_{measured} x\left[1 - \frac{({}^{40}Ar/{}^{36}Ar)_{air}}{({}^{40}Ar/{}^{36}Ar)_{measured}}\right] \qquad (1)$$

Air corrected ^{40}Ar constitutes 93.3% to 98.6% of the ^{40}Ar measured in Bravo Dome. Due to the correlation between crust and mantle ratios within the field, the mantle and crust contributions to ^{40}Ar can be resolved using the methods outlined in section 4.4.

Air corrected ^{40}Ar concentrations from Sheep Mountain vary from 1.30 x10^{-4} to 2.04 x 10^{-4} cm^{3}STP (^{40}Ar)/cm^3, constituting 89.5% to 98.7% of the total ^{40}Ar. As there is not a consistent variation in the crust and mantle ratios within the field contributions of $^{40}Ar_{mantle}$ and $^{40}Ar_{crust}$ cannot be resolved. Therefore air corrected ^{40}Ar must be considered in terms of $^{40}Ar_{crust+mantle}$.

4.4. Resolving Mantle and Crust Components

4.4.1. Bravo Dome

As previously outlined the distinct isotopes of Ne can be used to resolve the air, crust and mantle components from any sample. This enables the resolved $^{21}Ne_{air}$ component to be subtracted from the $^{21}Ne_{total}$, leaving 'air-corrected' $^{21}Ne_{crust+mantle}$. Plotting $^{21}Ne_{crust+mantle}/^{4}$He against ^{3}He/^{4}He (which has a negligible air component) defines a simple two-component mixing line (Fig. 6. (a)). This can be extrapolated to the well defined crustal ^{3}He/^{4}He endmember of 0.005 Ra [39] allowing the local ^{4}He/$^{21}Ne_{crust}$ input value to be resolved as 3.47 ± 0.24 x 10^{7}, when a ^{20}Ne/$^{22}Ne_{mntl}$ ratio of 12.5 is used [12]. The estimate of the mantle Ne endmember within the Bravo Dome field has been recently refined by Holland

and Ballentine (2006) to be 12.49 ± 0.04 for $^{20}Ne/^{22}Ne$ and 0.0578 ± 0.0003 for $^{21}Ne/^{22}Ne$.

This $^{4}He/^{21}Ne_{crust}$ value can then be used with the resolved $^{21}Ne_{crust}$ to calculate the crustal contributions to ^{3}He and ^{4}He, allowing a $^{3}He/^{4}He_{mantle}$ value to be calculated for each sample. The $^{3}He/^{4}He_{mantle}$ ratio determined in three samples have propagated errors which are less than 50% and these provide an error-weighted average of 5.35 ± 0.36 to 7.4 ± 0.5 Ra for the $^{3}He/^{4}He_{mantle}$ end member. A range of $^{4}He/^{21}Ne^{*}_{mantle}$ values can be derived by using the resolved $^{4}He_{mantle}$ with the amount of $^{21}Ne^{*}_{mantle}$, which has been corrected for solar contributions using the method outlined by Graham (2002).

A plot of $^{40}Ar_{crust+mantle}/^{4}He$ plotted against $^{3}He/^{4}He$ also generates a two component mixing line allowing the $^{4}He/^{40}Ar_{crust}$ input value to be determined (Fig. 6(b)). Extrapolation to the $^{3}He/^{4}He_{mantle}$ value determined above provides the range of resolved $^{40}Ar/^{4}He_{mantle}$ ratios and allows mantle and crust contributions to be corrected from the air corrected $^{40}Ar_{crust + mantle}$.

4.4.1. Sheep Mountain

The variation of $^{3}He/^{4}He$ ratios in the Sheep Mountain field is insufficient to allow extrapolation to the crustal $^{3}He/^{4}He$ end member and therefore the technique outlined for Bravo Dome cannot be applied. This means that the crustal input values in the field can not be determined directly. However, we have developed a method to constrain the range of mantle $^{3}He/^{4}He$, $^{4}He/^{21}Ne^{*}$, $^{3}He/^{22}Ne$, $^{4}He/^{40}Ar$ and $^{21}Ne^{*}/^{40}Ar$ values within the field using chi-squared minimization techniques.

As previously mentioned, $^{21}Ne_{crust}$ abundance can be determined using the air, crust and mantle Ne end members. Assuming a MORB-like mantle source of 8 Ra for the well gases allows the $^{20}Ne/^{22}Ne_{mantle}$ and $^{21}Ne/^{22}Ne_{mantle}$ values of 12.5 value and 0.06 to be used [12, 13, 40]). Note that three samples close to air are not used (2-9-H, 1-15-C and 5-15-O) because the crust and mantle components cannot be resolved.

The range exhibited in the $^{4}He/^{20}Ne$ ratios from Sheep Mountain of 3200 to 71100, is significantly above the air ratio value of 0.032 [41]. Therefore, the $^{3}He/^{4}He$ ratio can be considered as a sum of only two components, the crust and the mantle. The contribution of ^{4}He from the crust can be calculated for different $^{3}He/^{4}He_{mantle}$ ratios using the following formula [40]

$$\left[{}^{4}He\right]_{crust} = \frac{\left[{}^{4}He\right]_{tot} x\left[\frac{{}^{3}He}{{}^{4}He}\right]_{mntl} - \left[\frac{{}^{3}He}{{}^{4}He}\right]_{meas}}{\left[\frac{{}^{3}He}{{}^{4}He}\right]_{mntl} - \left[\frac{{}^{3}He}{{}^{4}He}\right]_{crust}} \qquad (2)$$

As the $^{4}He_{crust}$ is dependent on the $^{3}He/^{4}He_{mantle}$ end member, so too is the $^{4}He/^{21}Ne_{crust}$ ratio. Hence, for each sample, $^{4}He/^{21}Ne_{crust}$ values can be determined as the $^{3}He/^{4}He_{mantle}$ ratio is changed, allowing an error-weighted mean $^{4}He/^{21}Ne_{crust}$ ratio to be calculated from the dataset. Variable correction on each sample for the mantle component will leave varying crustal $^{4}He/^{21}Ne_{crust}$ residues. If we make the assumption that the field has been subjected to a constant crustal $^{4}He/^{21}Ne_{crust}$ input, then we would expect the 'correct' mantle $^{3}He/^{4}He$ value to exhibit the least deviation of the residual $^{4}He/^{21}Ne_{crust}$ from the

error weighted mean value. We can then use a χ^2 minimization to determine the 'correct' mantle $^3He/^4He_{mantle}$ end member and confidence limits on this determination provide an assessment of the statistical significance of the fit. Fig. 7. shows the χ^2 minimization for the $^3He/^4He_{mantle}$ range of 1 to 8 Ra. Whilst the dataset exhibits a minimization at 1.96 Ra, the χ^2_{min} value of 123.20 is very high and implies there is another variable in the dataset which is not being accounted for in the minimization.

As the resolved $^3He/^4He_{mantle}$ ratio is significantly below that of MORB we investigate the possibility that using the mantle Ne end members corresponding to an 8 Ra mantle source is inappropriate for low $^3He/^4He$ model values. As previously mentioned many helium isotope studies have identified that the isotopic ratio of helium within the SCLM is more radiogenic than that of the mid ocean ridge (MORB) source mantle. Gautheron et al., (2005) have recently proposed that this observation could be accounted for by closed system radiogenic production of noble gases, specifically ^4He, ^{21}Ne and ^{40}Ar within the mantle. This work also inferred that the Ne systematics of the SCLM beneath Europe is also more radiogenic than that of MORB.

Radiogenic ingrowth in the mantle source could also account for the low $^3He/^4He_{mantle}$ ratio resolved in the Sheep Mountain reservoir. In order to test this theory we have modelled the increase in $^{21}Ne/^{22}Ne$ ratios which will result from radiogenic production of ^{21}Ne, which will be proportional to the amount of ^4He required to reduce the $^3He/^4He_{mantle}$ ratio from 8 Ra to 2 Ra. This can be achieved as the ^3He concentration of the convecting mantle is known, from a

combination of the ^{3}He flux from mid ocean ridge basalts and MORB popping rock measurements, to be 4.4 x 10^{-11} $cm^{3}STPg^{-1}$ [42], assuming 10% partial melting [43]. Using the MORB $^{3}He/^{4}He$ ratio of 8 Ra, the ^{4}He concentration of the convecting mantle is 3.93 x 10^{-6} $cm^{3}STPg^{-1}$. Combining this with the measured $^{4}He/^{21}Ne^{*}$ value of MORB of 1.68 x 10^{7} gives a $^{21}Ne^{*}$ concentration of 2.34 x 10^{-13} $cm^{3}STPg^{-1}$. Therefore, the amount of ^{4}He required to reduce the $^{3}He/^{4}He_{mantle}$ ratio by radiogenic ingrowth can be calculated. This can be combined with estimates of the present day $^{4}He/^{21}Ne^{*}$ production rates in the mantle which vary between 2.22 x 10^{7} [44] and 2.79 x 10^{7} [45] to determine the amount of ^{21}Ne produced which is directly proportional to the quantity of radiogenic ^{4}He excess implied by the lower $^{3}He/^{4}He_{mantle}$ ratio. Adding this to the original ^{21}Ne concentration of the mantle, allows the $^{21}Ne/^{22}Ne_{mantle}$ ratio which corresponds to the lower $^{3}He/^{4}He_{mantle}$ ratio to be determined (Fig. 8.). Although we have used current estimates of mantle noble gas concentrations, it should be noted that the increase in $^{21}Ne/^{22}Ne$ corresponding to the reduction in $^{3}He/^{4}He_{mantle}$ ratios is only dependent on the $^{4}He/^{21}Ne$ mantle production ratio and is therefore independent of absolute concentrations.

Using exactly the same method as previously outlined we can perform a χ^{2} minimization for lower $^{3}He/^{4}He_{mantle}$ values, but this time coupled with the change in mantle $^{21}Ne/^{22}Ne$ end member. We perform this minimization for both estimates of $^{4}He/^{21}Ne_{mantle}$ production.

Both minimizations produce low χ^{2}_{min} values indicating a statistically significant resolution of the $^{3}He/^{4}He_{mantle}$ ratio using the two $^{4}He/^{21}Ne_{mantle}$ production values. This conclusively shows that radiogenic production within the SCLM source,

responsible for supplying volatiles to the field, is reducing both the $^{3}He/^{4}He_{mantle}$ ratio and causing a corresponding increase in the $^{21}Ne/^{22}Ne_{mantle}$ end member. The two minimizations give a range of values for $^{3}He/^{4}He_{mantle}$ of 2.59 ± 0.15 to 3.00 ± 0.18, and a corresponding range of $^{4}He/^{21}Ne_{mantle}$ values of 2.90 ± 0.29 and 3.09 ± 0.32 x 10^{7}, respectively (Fig. 9. & 10.). Confidence in this procedure is reinforced by the fact that resolved $^{4}He/^{21}Ne_{crust}$ values are remarkably similar to those measured in Bravo Dome.

Using the derived range of $^{3}He/^{4}He_{mantle}$ values, a similar χ^2 minimization can be performed for a range of $^{4}He/^{40}Ar_{mntl}$ ratios, allowing the mantle He/Ar ratio of the Sheep Mountain field to be determined. As the $^{40}Ar_{crust}$ is dependent on the $^{4}He/^{40}Ar_{mantle}$ end member, so too is the $^{21}Ne/^{40}Ar_{crust}$ ratio. Therefore, for each sample, $^{21}Ne/^{40}Ar_{crust}$ values can be determined as the $^{4}He/^{40}Ar_{mantle}$ ratio is changed. This allows an error-weighted mean $^{21}Ne/^{40}Ar_{crust}$ ratio to be calculated from the dataset. If we assume that the field has been subjected to a constant crustal $^{21}Ne/^{40}Ar_{crust}$ input, similar to the assumption made for $^{4}He/^{21}Ne_{crust}$, then the 'correct' mantle $^{4}He/^{40}Ar_{mntl}$ end member should result in the least deviation in $^{21}Ne/^{40}Ar_{crust}$ values from the error-weighted mean. This minimization is shown in Fig. 11. and enables us to derive a $^{4}He/^{40}Ar_{mantle}$ range of 0.85 – 1.00. Multiplication of the inverse of the $^{4}He/^{21}Ne_{mantle}$ range with the $^{4}He/^{40}Ar_{mantle}$ values allows the range of $^{21}Ne/^{40}Ar_{mantle}$ values to be derived. All of the resolved mantle ratio ranges are documented in Table 3.

Plots of $^{36}Ar_{total}/^{3}He$ and $^{84}Kr_{total}/^{3}He$ versus $^{4}He/^{3}He$ from the Bravo Dome field produce pseudo-two-component mixing trends that can be extrapolated to the mantle $^{4}He/^{3}He$ value. This allows a range of $^{36}Ar_{mantle}$ and $^{84}Kr_{mantle}$ components

to be resolved from the $^{36}Ar_{crust+air}$ and $^{84}Kr_{crust+air}$ contributions. However, due to the lack of variation in $^{4}He/^{3}He$ ratios in the Sheep Mountain field, this technique cannot be used and therefore mantle contributions to ^{36}Ar and ^{84}Kr cannot be resolved from the air and crust components.

5. DISCUSSION

Within the Sheep Mountain field we observe a significant reduction in the $^{3}He/^{4}He_{mantle}$ ratio which we can attribute to radiogenic production in the mantle. This can be resolved by modelling a correlated increase of the $^{21}Ne/^{22}Ne$ mantle end member with a lowering of the $^{3}He/^{4}He_{mantle}$ ratio. We now consider the resolved mantle ratios, specifically $^{3}He/^{22}Ne_{mantle}$, $^{4}He/^{21}Ne^{*}_{mantle}$, $^{4}He/^{40}Ar_{mantle}$ and $^{21}Ne/^{40}Ar_{mantle}$.

5.1. Resolved Mantle Components

5.1.1. $^{3}He/^{4}He_{mantle}$ and $^{3}He/^{22}Ne_{mantle}$ ratios

Firstly we investigate the relationship between $^{3}He/^{4}He_{mantle}$ and the elemental $^{3}He/^{22}Ne_{mantle}$ ratio. As neither isotope is significantly produced by radiogenic mechanisms, the measured ratio should be unaffected by the radiogenic lowering of the $^{3}He/^{4}He_{mantle}$ ratio within the gas fields. It is therefore significant that the resolved range of $^{3}He/^{22}Ne_{mantle}$ in both fields is considerably lower than that of MORB (Fig. 12). This implies that there is a process in addition to radiogenic ingrowth which is fractionating the $^{3}He/^{22}Ne_{mantle}$ ratio in both fields. In the Bravo Dome field values vary from 2.56 to 2.77, 1.8 - 1.9 times lower than the measured MORB popping rock value of 4.90 [42, 46].

Importantly, the small range of resolved $^{3}He/^{22}Ne_{mantle}$ ratios in Sheep Mountain of 2.80 – 2.81 ± 0.16 is indistinguishable from the range of values resolved in Bravo Dome and is also 1.75 times lower than the MORB value. This shows that the Sheep Mountain field, after correction for radiogenic production in the mantle

by use of a higher $^{21}Ne/^{22}Ne$ end member, has an identical elemental $^{3}He/^{22}Ne_{mantle}$ ratio to that of Bravo Dome. This implies that a similar process could be responsible for lowering the $^{3}He/^{22}Ne_{mantle}$ in both fields.

5.1.2. Equilibrium Partitioning

Previous studies have shown that equilibrium partitioning of He and Ne between a melt and gas phase can decrease the He/Ne ratio in the gas phase [47, 48]. The magnitude of this fractionation, $F[He/Ne]_{gas}$, is defined by the He/Ne ratio in the gas phase, $[He/Ne]_{gas}$, divided by the original He/Ne ratio in the melt, $[He/Ne]_{melt}$, prior to the formation of the gas phase. Equilibrium partitioning between He and Ne can be modelled using their respective Henry's solubility constants. The absolute solubilities of noble gases in a silicate melt are only weakly affected by temperature and are therefore typically calculated as a function of the percentage ionic porosity [49]. When the gas/melt volume ratio approaches zero, He and Ne in the gas phase are fractionated proportionally to their relative solubilities in the melt and $F(He/Ne)_{gas}$ reaches a maximum (where $F[He/Ne]_{gas} \rightarrow K_{Ne}/K_{He}$ when K_{He} and K_{Ne} are the respective Henry coefficients for He and Ne). Fig. 4.13. shows the maximum $F[He/Ne]_{gas}$ against percent ionic porosities of 45 – 52%.

The amount of fractionation which has affected the well gas samples can be calculated by comparing the values resolved in each field with the theoretical and observed mantle production ranges. Assuming initial MORB mantle values of 4.9 for $^{3}He/^{22}Ne_{mantle}$, the $F[He/Ne]$ value required to account for the $^{3}He/^{22}Ne_{mantle}$ ratio range of 2.80 - 2.81 measured in the Sheep Mountain field is

~0.57, almost identical to the *F*[He/Ne] values of between 0.52 and 0.56 required to produce the Bravo Dome range of 2.56 – 2.77. These fractionation factors can be accounted for by ionic porosity in the degassing melt of ~48.3% for both fields (Fig. 13). Ionic porosity is crudely anti-correlated to melt density and a melt density of 2.6 g cm^{-3}, can account for the derived ionic porosity, provided that the gas/melt ratio is small. Higher ionic porosities and lower melt densities than these cannot account for the minimum fractionation observed within the fields. These values are comparable with the lower end of the density range of typical mafic melts (10 - 20% partial melt) of 2.6 - 2.7 g cm^{-3} [48].

5.1.3. $^{3}He/^{4}He_{mantle}$ and $^{4}He/^{21}Ne^{*}_{mantle}$ ratios

As radiogenic ingrowth of ^{4}He can account for the reduction of the Sheep Mountain $^{3}He/^{4}He_{mantle}$ ratios, the amount of ^{4}He required to lower the values measured in the field can be easily calculated. Using the known mantle production ratios for $^{4}He/^{21}Ne^{*}$ and $^{4}He/^{40}Ar$ enables the amount of ^{21}Ne and ^{40}Ar corresponding to this ^{4}He to also be calculated. This allows a range of predicted $^{4}He/^{21}Ne^{*}_{mantle}$, $^{4}He/^{40}Ar_{mantle}$ and $^{21}Ne^{*}/^{40}Ar_{mantle}$ ratios that correspond to the $^{3}He/^{4}He_{mantle}$ reduction to be determined. In the Bravo Dome field the highest $^{3}He/^{4}He_{mantle}$ ratio value measured of 7.40 Ra is extremely close to that of MORB and therefore radiogenic production should not significantly alter the $^{4}He/^{21}Ne^{*}_{mantle}$ ratio. Applying the same methodology to the Sheep Mountain field, the reduction of the $^{3}He/^{4}He_{mantle}$ ratio to between 2.59 and 3.00 Ra would result in an increase of the $^{4}He/^{21}Ne^{*}_{mantle}$ ratio to between 2.01 - 2.30 x 10^{7} and 1.98 – 2.24 x 10^{7}, respectively.

However, the actual $^{4}He/^{21}Ne^{*}_{mantle}$ range resolved in the Bravo Dome field of 1.23 - 1.45 x 10^{7} is between 1.2 to 1.4 times lower than the measured MORB popping rock value. $^{4}He/^{21}Ne^{*}_{mantle}$ ratios resolved in the Sheep Mountain field range from 1.03 ± 0.06 to 1.19 ± 0.07 x 10^{7}, between 1.4 to 1.6 times lower than the MORB value and only slightly below the Bravo Dome value (Fig. 14.).

This reduction could be explained by the same phase partitioning process outlined to account for the reduction in $^{3}He/^{22}Ne_{mantle}$ ratios. Applying the same maximum fractionation factor of 0.52 observed in the $^{3}He/^{22}Ne_{mantle}$ ratios produces two fractionation lines which can directly account for the range of values measured in Sheep Mountain (Fig. 14.) The resolved range in Bravo Dome, however, is somewhat above the predicted line, implying that fractionation of the $^{4}He/^{21}Ne^{*}_{mantle}$ ratio has not been as severe as that observed in the $^{3}He/^{22}Ne_{mantle}$ ratios from the field.

5.1.4. $^{3}He/^{4}He_{mantle}$, $^{4}He/^{40}Ar_{mantle}$ and $^{21}Ne/^{40}Ar_{mantle}$

The radiogenic production ratio of $^{4}He/^{40}Ar_{mantle}$ is ~3 [39]. Using this value with the calculated ^{4}He concentration that corresponds to the individual $^{3}He/^{4}He_{mantle}$ values and the MORB value allows us to predict the increase of the $^{4}He/^{40}Ar_{mantle}$ values that would result from radiogenic production in the mantle (Fig. 15). It can be clearly seen that the $^{4}He/^{40}Ar_{mantle}$ ratios measured in the fields are considerably lower than both MORB and the predicted $^{4}He/^{40}Ar_{mantle}$ fractionation trend, implying that radiogenic production alone cannot account for the Bravo Dome and Sheep Mountain values.

However, as previously outlined, phase fractionation between a gas and melt can account for the lower He/Ne ratios measured in both fields. It is therefore probable that a similar process could be responsible for the reduction of the He/Ar ratios. As Ar is considerably less soluble in a melt than Ne, it is more readily degassed from the melt, resulting in a higher degree of fractionation within the He/Ar ratios of the exsolved gas [49]. This results in a high *F*[He/Ar] value of 0.19 as opposed to the F[He/Ne] value of 0.52 for a melt with an ionic porosity of 48.3% (Fig. 13.). However, this degree of fractionation is too severe to account for the $^{4}He/^{40}Ar_{mantle}$ ratios resolved in both gas fields (Fig. 15.). This implies that there is an additional fractionation process acting on the noble gases within the field.

The model outlined by Gilfillan et al., (2006a) could provide an additional process to account for the fractionation observed in the fields. In this model magmatic degassing emplaces mantle derived CO_2 and noble gases into the groundwater in the gas fields. Both are subsequently degassed from the groundwater upon reaching the gas/groundwater contact. This degassing process will result in an increase in the He/Ar ratios as He is less soluble than Ar in water and is therefore preferentially degassed from the groundwater. For the conditions in the Sheep Mountain field the predicted *F*[He/Ar] for this process is 2.11 and within for Bravo Dome the predicted *F*[He/Ar] is 2.55. The trends that would result from this fractionation are also plotted on Fig. 15. and importantly they can account for the range of $^{4}He/^{40}Ar_{mantle}$ values observed in both fields. Given that this process can account for the He/Ar ratios in both fields, the effect on the He/Ne ratios must also be considered. As the solubility of He and Ne in

water is extremely similar [50] the F[He/Ne] under the reservoir conditions in Sheep Mountain and Bravo Dome will be 1.05 and 1.09, respectively, and therefore the groundwater degassing process will not significantly altered the He/Ne_{mantle} ratios in the fields.

Importantly, using exactly the same model, the resolved range of $^{21}Ne/^{40}Ar_{mantle}$ values from Sheep Mountain and the lower value from Bravo Dome can be accounted for (Fig. 16). However, the upper values resolved in Bravo Dome for both the $^{4}He/^{40}Ar_{mantle}$ and $^{21}Ne/^{40}Ar_{mantle}$ ratios are less fractionated compared with the Popping Rock value than this model predicts. This corresponds to the high $^{3}He/^{4}He_{mantle}$ value of 7.40 ± 0.50 which is within the lower range of MORB, suggesting that the He/Ar and Ne/Ar ratios of the mantle rich portion of the Bravo Dome field are not significantly fractionated from MORB. At the moment it is unclear as to why the resolved $^{3}He/^{22}Ne_{mantle}$ ratios in this portion are significantly lower whilst these values are not.

5.2. Implications to models of SCLM evolution

5.2.1. Mantle Plume Model

It has been suggested that a mantle plume could be the primary cause of the Cenozoic volcanism and associated high heat flow in the southwest US [23]. Several workers have also proposed that the Colorado Plateau uplift event could be explained by the presence of a mantle plume [22, 25]. This has been strongly argued against by Dodson et al. (1998) and we support this argument. There is no evidence of a primitive high $^{3}He/^{4}He_{mantle}$ component within our data such as that observed in Yellowstone or Hawaii, and in fact, our derived $^{3}He/^{4}He_{mantle}$

values from the Sheep Mountain field are significantly more radiogenic than those of MORB. This is reinforced by data from extensional regions around the world including Europe [1, 3, 4, 51], continental Cameroon Line [9], East African Rift and Canada [52].

5.2.2. Closed system evolution of MORB mantle

Our results highlight that closed system radiogenic production can account for the low $^{3}He/^{4}He_{mantle}$ ratios resolved from the Sheep Mountain field. Closed system radiogenic ingrowth models for the south-western US have been previously proposed by both Reid and Graham (1996) and Dodson et al. (1998). Reid and Graham concluded that the lithospheric mantle in the region is not a highly degassed reservoir contaminated by He derived from the asthenosphere. Rather they believe that it is a reservoir which has a slightly elevated $(U+Th)/^{3}He$ ratio (and therefore lower $^{3}He/^{4}He$ ratios) compared to the depleted upper mantle source, which has remained unmodified for 1.7 Ga. The $^{3}He/^{4}He_{mantle}$ ratio range resolved in our sample suite of 2.59 – 3.00 Ra can be explained by radiogenic production of between 6.55 to 8.26 x 10^{-6} $cm^{3}STP/g$ of ^{4}He, assuming an initial mantle ratio of 8 Ra and a $^{4}He_{mantle}$ concentration of 3.93 x 10^{-6}. Using the present day mantle ^{4}He production ratio of 4.13 x 10^{-15} $cm^{3}STP/g$ per year [39] requires that the upper mantle source has been isolated for a period of 1.59 - 1.99 Ga, comparing favourably with the value derived by Reid and Graham (1996).

However, our results also advocate that closed system radiogenic ingrowth is not the only process required to account for mantle ratios measured. For the first

time we have been able to resolve both the mantle He/Ne ratios and the He/Ar ratios of the SCLM source. Importantly, in both the Sheep Mountain and Bravo Dome fields, both of these isotope pairs are depleted relative to the MORB mantle values. This can only be explained by partial degassing of small melt fractions from asthenospheric melts that have been emplaced into the SCLM after radiogenic ingrowth.

6. CONCLUSIONS

We have identified that reduction of $^{3}He/^{4}He_{mantle}$ ratio within the Sheep Mountain gas field in central Colorado can be attributed to radiogenic production within the SCLM. Using a χ^2 minimization on the variation of derived $^{4}He/^{21}Ne_{crust}$ ratios within the field, combined with a radiogenically raised $^{21}Ne/^{22}Ne_{mantle}$ end member we have resolved $^{3}He/^{4}He_{mantle}$ ratios of 2.59 ± 0.15 to 3.00 ± 0.18 Ra within the field. These values correspond with $^{21}Ne/^{22}Ne_{mantle}$ values of 0.135 and 0.121, respectively. Using these $^{3}He/^{4}He_{mantle}$ end member values with $^{21}Ne_{mantle}$ values resolved from Ne three component analysis, has enabled a derivation of the elemental $^{3}He/^{22}Ne_{mantle}$ and radiogenic $^{4}He/^{21}Ne^{*}_{mantle}$ ratios. A second χ^2 minimization performed on the variation of $^{21}Ne/^{40}Ar_{crust}$ ratios has allowed us to also determine both the $^{4}He/^{40}Ar_{mantle}$ and $^{21}Ne/^{40}Ar_{mantle}$ ratios within the field.

Using the known mantle production ranges for $^{4}He/^{21}Ne$ and $^{4}He/^{40}Ar$ has allowed us to predict the radiogenic He/Ne and He/Ar ratios that correspond to the radiogenically lowered $^{3}He/^{4}He_{mantle}$ ratios. Comparing these values with those resolved from both the Sheep Mountain field and the Bravo Dome field located in north western New Mexico by Ballentine (2005) has allowed us to

identify a clear and coherent depletion of He to Ne and He to Ar. This depletion can only be explained by partial degassing of small melt fractions from asthenospheric melts which have been emplaced into the SCLM. This is the first time that it has been possible to resolve and account for both the mantle He/Ne and He/Ar ratios within the SCLM source. We can also rule out the involvement of any plume component in the mantle source of the two gas fields and therefore also any plume influence on the Colorado Plateau Uplift event.

Acknowledgements

This research has been supported by the National Environmental Research Council. We thank BP and Larry Nugent for permission to sample at Sheep Mountain, Oxy for permission to sample Bravo Dome and Advanced Resources International, USA for their assistance in the field and in providing background information. Greg Holland, Joanna Mount and David Murphy are also thanked for useful discussions on the subject.

References

[1] C. Gautheron, M. Moreira, Helium signature of the subcontinental lithospheric mantle, Earth and Planetary Science Letters 199(2002) 39.

[2] D.R. Porcelli, J.O.H. Stone, R.K. O'Nions, Enhanced $^{3}He/^{4}He$ ratios and cosmogenic helium in ultramafic xenoliths, Chemical Geology 64(1987) 25.

[3] T.J. Dunai, H. Baur, Helium, neon, and argon systematics of the European subcontinental mantle: Implications for its geochemical evolution, Geochimica et Cosmochimica Acta 59(1995) 2767.

[4] T.J. Dunai, D.R. Porcelli, Storage and transport of noble gases in the subcontinental lithosphere, in: D.R. Porcelli, C.J. Ballentine, R. Weiler, (Eds), Noble gases in Geochemistry and Cosmochemistry, Reviews in Mineralogy & Geochemistry, 2002, pp. 371-409.

[5] M.R. Reid, D.W. Graham, Resolving lithospheric and sub-lithospheric contributions to helium isotope variations in basalts from the southwestern US, Earth and Planetary Science Letters 144(1996) 213.

[6] R.S. White, D. McKenzie, Mantle plumes and flood basalts, Journal of Geophysical Research 108(1995) 17543 - 17585.

[7] R.A. Duncan, M.A. Richards, Hotspots, mantle plumes, flood basalts and true polar wander, Reviews of Geophysics 29(1991) 31 - 50.

[8] T. Matsumoto, M. Honda, I. McDougall, S.Y. Reilly, Noble gases in anhydrous lherzolites from the newer volcanics, southeastern Australia: a MORB-like reservoir in the subcontinental mantle, Geochimica et Cosmochimica Acta 62(1998) 2521.

[9] D.N. Barford, C.J. Ballentine, A.N. Halliday, J.G. Fitton, Noble gases inthe Cameroon line and the He, Ne and Ar isotopic composition of high y (HIMU) mantle, Journal of Geophysical Research 104(1999) 29509-29527.

[10] D. Seber, M. Barazangi, A. Ibenbrahim, A. Demnati, Geophysical evidence for lithospheric delamination beneath the Alboran Sea and Rif-Betic mountains, Nature 379(1996) 785-790.

[11] A. Dodson, D. DePaolo, B. Kennedy, Helium isotopes in lithospheric mantle: Evidence from Tertiary basalts of the western USA, Geochimica et Cosmochimica Acta 62(1998) 3775-3787.

[12] C.J. Ballentine, B. Marty, B.S. Lollar, M. Cassidy, Neon isotopes constrain convection and volatile origin in the Earth's mantle, Nature 433(2005) 33-38.

[13] G. Holland, C.J. Ballentine, Breaking the noble gas subduction barrier, Nature 441(2006) 186-191.

[14] M.S. Boulos, O.K. Manuel, Xenon Record Of Extinct Radioactivities In Earth, Science 174(1971) 1334-.

[15] W.A. Butler, P.M. Jeffery, J.H. Reynolds, Isotopic Variations In Terrestrial Xenon, Journal Of Geophysical Research 68(1963) 3283-.

[16] M.W. Caffee, G.U. Hudson, C. Velsko, G.R. Huss, E.C. Alexander, A.R. Chivas, Primordial noble cases from Earth's mantle: Identification of a primitive volatile component, Science 285(1999) 2115-2118.

[17] E.W. Hennecke, O.K. Manuel, Noble gases in CO_2 Well Gas, Harding County, New-Mexico, Earth And Planetary Science Letters 27(1975) 346-355.

[18] D. Phinney, J. Tennyson, U. Frick, Xenon In CO_2 Well Gas Revisited, Journal of Geophysical Research 83(1978) 2313-2319.

[19] S.P. Smith, J.H. Reynolds, Excess ^{129}Xe In a Terrestrial Sample as Measured in a Pristine System, Earth and Planetary Science Letters 54(1981) 236-238.

[20] T. Staudacher, Upper Mantle Origin For Harding County Well Gases, Nature 325(1987) 605-607.

[21] R.E. Zartman, J.H. Reynolds, G.J. Wasserburg, Helium argon, and carbon in some natural gases, Journal of Geophysical Research 66(1961) 277-306.

[22] T. Parsons, J. McCarthy, The active southwest margin of the Colorado Plateau: uplift of mantle origin, Geological Society of America Bulletin 107(1995) 139-147.

[23] J.G. Fitton, D. James, W.P. Leeman, Basic Magmatism Associated with Late Cenozoic Extension in the Western United-States - Compositional Variations in Space and Time, Journal of Geophysical Research-Solid Earth and Planets 96(1991) 13693-13711.

[24] Y. Dilek, E.M. Moores, A Tibetan model for the early Tertiary western United States, J. Geol. Soc. 156(1999) 929-941.

[25] J.T. Wilson, Mantle plumes and plate motions, Tectonophysics 19(1973) 149-164.

[26] G.A. Thompson, M.L. Zoback, Regional geophysics of the Colorado Plateau, Tectonophysics 61(1979) 149-181.

[27] N. Beghoul, M. Barazangi, Mapping High Pn Velocity beneath the Colorado Plateau Constrains Uplift Models, Journal of Geophysical Research-Solid Earth and Planets 94(1989) 7083-7104.

[28] G. Zandt, S.C. Myers, T.C. Wallace, Crust and Mantle Structure across the Basin and Range Colorado Plateau Boundary at 37-Degrees-N Latitude and Implications for Cenozoic Extensional Mechanism, Journal of Geophysical Research-Solid Earth 100(1995) 10529-10548.

[29] R. Allis, T. Chidsey, W. Gwynn, C. Morgan, S. White, M. Adams, J. Moore, Natural CO_2 Reservoirs on the Colorado Plateau and Southern Rocky Mountains: Candidates for CO_2 sequestration, DOE/NETL: 1st National Conference of Carbon Sequestration. Procedings Volume(2001).

[30] L.A. Woodward, Geology and Hydrocarbon Potential of the Raton Basin, New Mexico, in: J.E. Fassett, (Ed), Oil and Gas Fields of the Four Corners Area 3, Four Corners Geological Society, 1983, pp. 789-799.

[31] R.B. Johnston, Geology of Huerferno Park Area, Huerferno and Custer County, Colorado, U.S. Geological Survey Bulletin No. 1071-D(1959).

[32] G. Roth, Sheep Mountain and Dike Mountain Fields, Huerfano County, Colorado; A source of CO_2 for enhanced oil recovery, in: J.E. Fassett, (Ed), Oil and Gas Fields of the Four Corners Area 3, Four Corners Geological Society, 1983, pp. 740-744.

[33] S.J. Baines, R.H. Worden, The long term fate of CO_2 in the subsurface: natural analogues for CO_2 storage, in: S.J. Bains, R.H. Worden, (Eds), Geological Storage of Carbon Dioxide, Special Publications 233, Geological Society, London, 2004, pp. 59-85.

[34] D.L. Baars, The Colorado Plateau: A Geologic History, University of New Mexico Press, 2000.

[35] R.E. Johnson, Bravo Dome carbon dioxide area, North east New Mexico, in: J.E. Fassett, (Ed), Oil and Gas Fields of the Four Corners area 3, Four Corners Geological Society, 1983, pp. 745-748.

[36] R.F. Broadhead, Natural accumulations of carbon dioxide in the New Mexico region - Where are they, how do they occur and what are the uses for CO_2? Lite Geology 20(1998) 2-6.

[37] C.J. Ballentine, M. Schoell, D. Coleman, B.A. Cain, 300-Myr-old magmatic CO2 in natural gas reservoirs of the west Texas Permian basin, Nature 409(2001) 327-331.

[38] B. Marty, A. Jambon, $C/^3He$ in volitile fluxes from the solid Earth: Implications for carbon geodynamics, Earth and Planetary Science Letters 83(1987) 16-26.

[39] C.J. Ballentine, P.G. Burnard, Production, release and transport of noble gases in the continental crust, in: D.R. Porcelli, C.J. Ballentine, R. Weiler, (Eds), Noble Gases in Geochemistry and Cosmochemistry, Reviews in Mineralogy & Geochemistry 47, 2002, pp. 481-538.

[40] C.J. Ballentine, R. Burgess, B. Marty, Tracing fluid origin, transport and interaction in the crust, in: D.R. Porcelli, C.J. Ballentine, R. Weiler, (Eds), Noble Gases in Geochemistry and Cosmochemistry, Reviews in Mineralogy & Geochemistry 47, 2002, pp. 539-614.

[41] R. Kipfer, W. Aeschbach-Gertig, F. Peeters, M. Stute, Noble gases in lakes and groundwaters, Noble Gases in Geochemistry and Cosmochemistry, Reviews in Mineralogy & Geochemistry 47, 2002, pp. 615-700.

[42] M. Moreira, J. Kunz, C. Allegre, Rare Gas Systematics in Popping Rock: Isotopic and Elemental Compositions in the Upper Mantle, Science 279(1998) 1178-1181.

[43] D.R. Porcelli, C.J. Ballentine, Models for the distribution of terrestrial noble gases and evolution of the atmosphere, Noble Gases in Geochemistry and Cosmochemistry, Reviews in Mineralogy & Geochemistry 47, 2002, pp. 411-480.

[44] I. Yatsevich, M. Honda, Production of Nucleogenic Ne in the Earth from Natural Radioactive Decay, Journal Of Geophysical Research, Solid Earth 102(1997) 10291-10298.

[45] I. Leya, R. Wieler, Nucleogeinc production of Ne isotopes in Earth's crust and upper mantle induced by alpha particles from the decay of U and Th., Journal of Geophysical Research, Solid Earth 104(1999) 15439-15450.

[46] P. Burnard, D. Graham, G. Turner, Vesicle-Specific Noble Gas Analyses of "Popping Rock": Implications for Primordial Noble Gases in Earth, Science(1997) 568-570.

[47] C.J. Ballentine, R.K. O'Nions, The nature of mantle neon contributions to Vienna Basin hydrocarbon reservoirs, Earth and Planetary Science Letters 113(1992) 553-567.

[48] C.J. Ballentine, Resolving the mantle He/Ne and crustal $^{21}Ne/^{22}Ne$ in well gases, Earth and Planetary Science Letters 152(1997) 233-249.

[49] M.R. Carroll, D.S. Draper, Noble gases as trace elements in magmatic processes, Chemical Geology 117(1994) 37-56.

[50] R. Crovetto, R. Fernandez-Prini, M. Laura Japas, Solubilities of inert gases and methane in H_2O and in D_2O in the temperature range of 300 to 600K, Journal of Chemical Physics 76(1982) 1077-1086.

[51] U. Gautheron, M. Moreira, C. Allegre, He, Ne and Ar composition of the European lithospheric mantle, Chemical Geology 217(2005) 97-112.

[52] J.M.D. Day, D.R. Hilton, D.G. Pearson, C.G. Macpherson, B.A. Kjarsgaard, P.E. Janney, Absence of a high time-integrated ^{3}He/(U+Th) source in the mantle beneath continents, Geology 33(2005) 733-736.

[53] D. Graham, Noble Gas Isotope Geochemistry of Mid-Ocean Ridge and Ocean Island Basalt: Characterization of Mantle Source Reservoirs, in: D. Porcelli, C.J. Ballentine, R. Wieler, (Eds), Noble Gases in Geochemistry and Cosmochemistry 47, 2002, pp. 247-317.

Figures

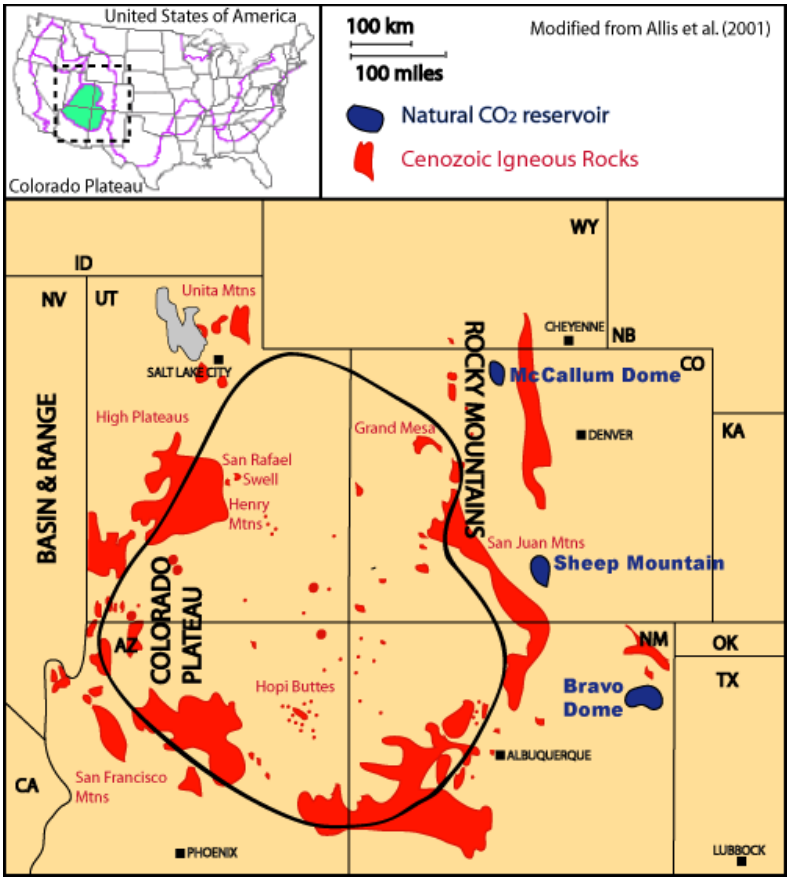

Fig. 1. Map of the Colorado Plateau illustrating the sites of major Cenozoic igneous provinces and the location of the natural CO_2 reservoirs sampled within the region.

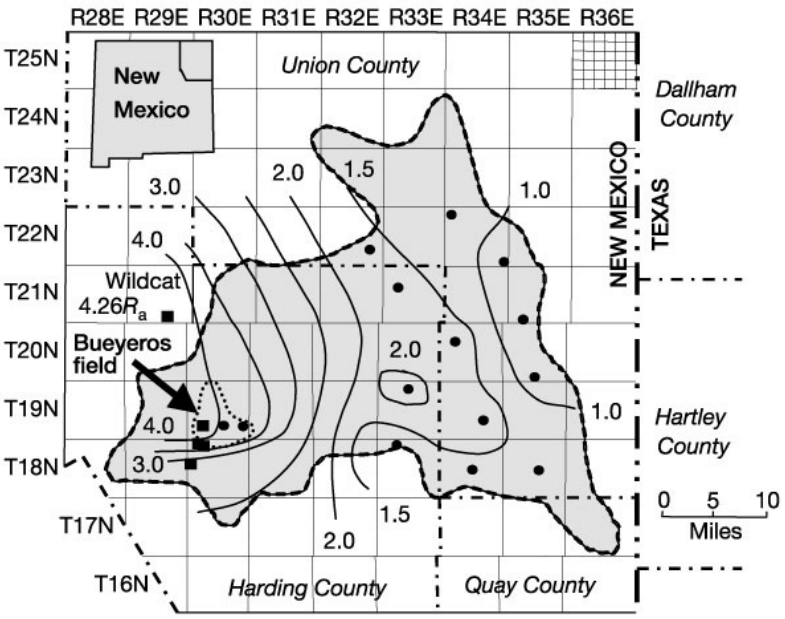

Fig. 2. Contour plot of coherent $^{3}He/^{4}He$ variation (R/Ra) observed in the Bravo Dome Field. Filled circles show locations of samples for this study, filled squares document non-producing wells and one wildcat well not reported, but used in the $^{3}He/^{4}He$ contouring (from Ballentine et al., 2005).

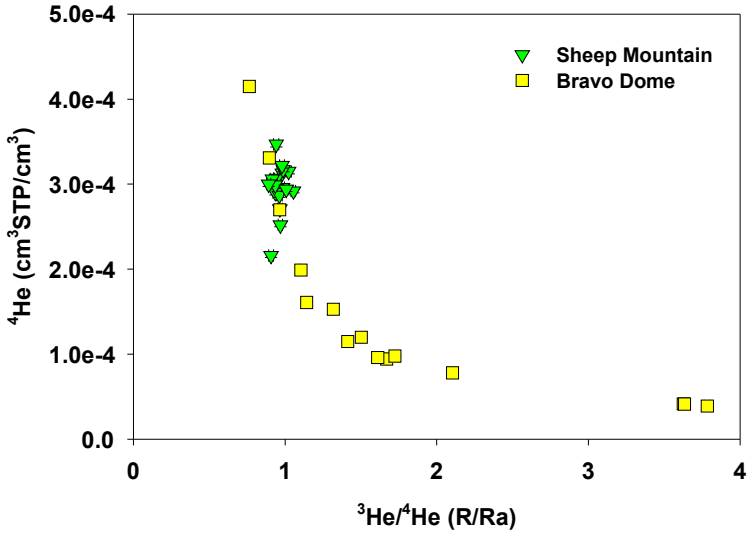

Fig. 3. Plot of $^{3}He/^{4}He$ (R/Ra) against ^{4}He concentration for the samples in this study. Bravo Dome $^{3}He/^{4}He$ ratios exhibit clear mixing between a high $^{3}He/^{4}He$ mantle end member and a low $^{3}He/^{4}He$ crust end member. Values within the Sheep Mountain field show minimal variation. Error bars are smaller than printed symbols.

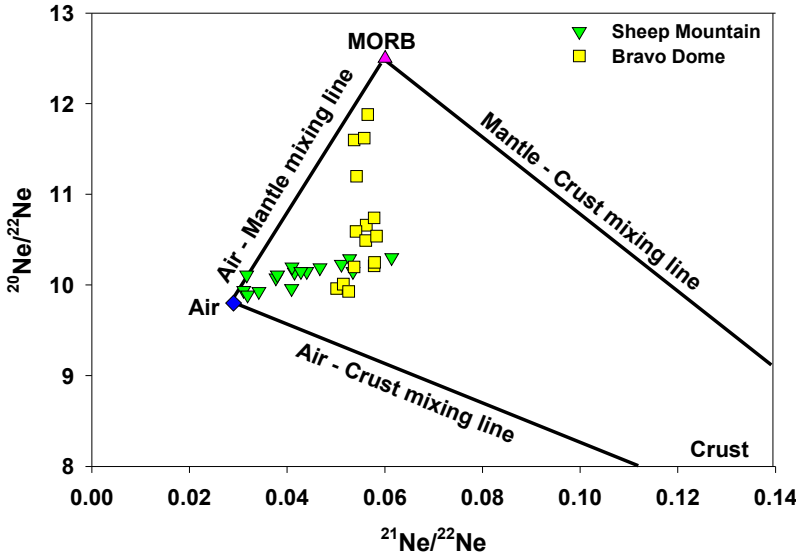

Fig. 4. Plot of $^{20}Ne/^{22}Ne$ ratio against $^{21}Ne/^{22}Ne$ for samples from Sheep Mountain and Bravo Dome. The plot highlights two distinct mixing trends; mixing between an air/crust mixture and the mantle, observed in Bravo Dome, and mixing between a mantle/crust mix and air, observed in Sheep Mountain.

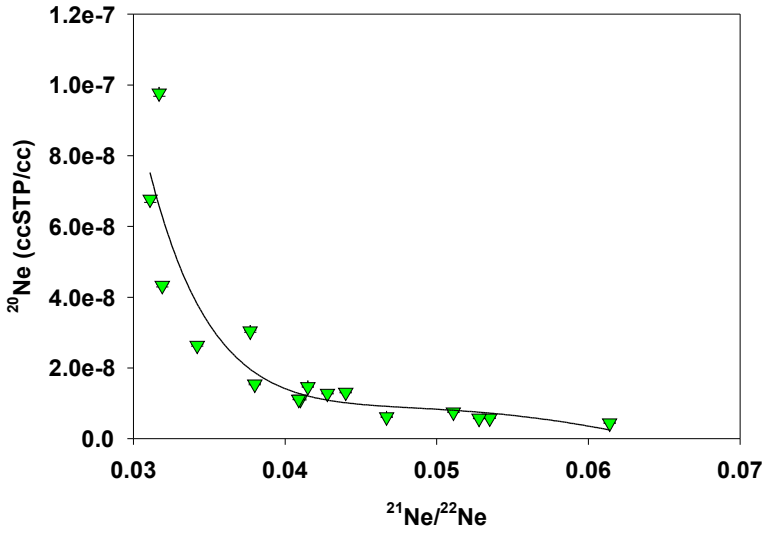
1.2e-7
1.0e-7
8.0e-8
6.0e-8
4.0e-8
2.0e-8
0.0
^{20}Ne (ccSTP/cc)
0.03
0.04
0.05
0.06
0.07
^{21}Ne/^{22}Ne

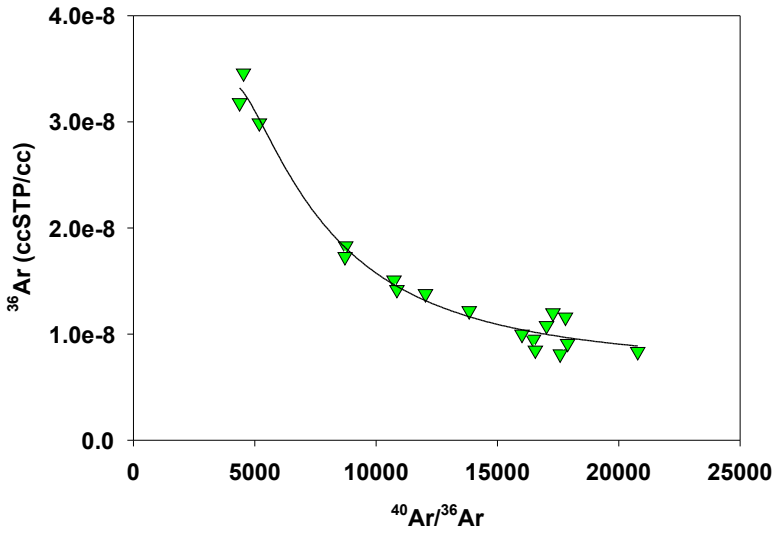
4.0e-8
3.0e-8
2.0e-8
1.0e-8
0.0
^{36}Ar (ccSTP/cc)
0
5000
10000
15000
20000
25000
^{40}Ar/^{36}Ar

Fig. 5. (a) top: Plot of ^{20}Ne (ccSTP/cc) against $^{21}Ne/^{22}Ne$ for samples from Sheep Mountain. **Fig. 5. (b) bottom:** Plot of ^{36}Ar (ccSTP/cc) against $^{40}Ar/^{36}Ar$ for samples from Sheep Mountain. Both plots highlight that of young groundwater containing a low concentration of crustal noble gases is responsible for reducing both the $^{21}Ne/^{22}Ne$ and $^{40}Ar/^{36}Ar$ ratios.

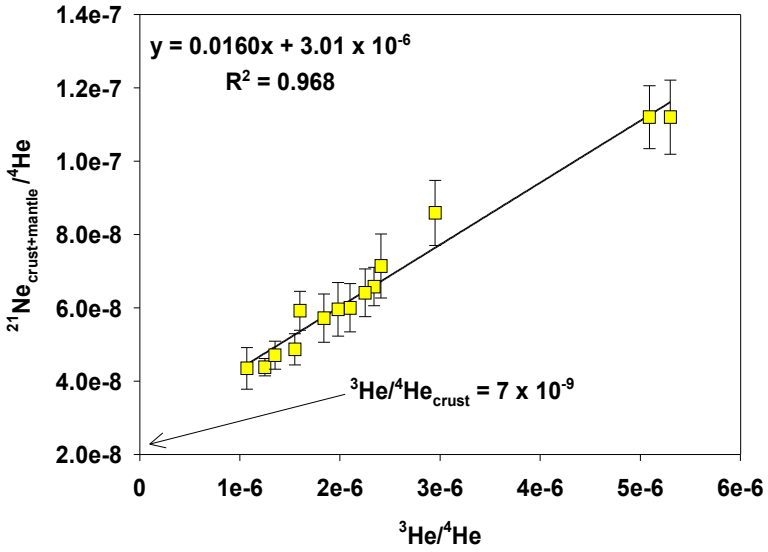
y = 0.0160x + 3.01 x 10-6
R2 = 0.968
3He/4Hecrust = 7 x 10-9
21Necrust+mantle/4He
3He/4He
1.4e-7
1.2e-7
1.0e-7
8.0e-8
6.0e-8
4.0e-8
2.0e-8
0
1e-6
2e-6
3e-6
4e-6
5e-6
6e-6

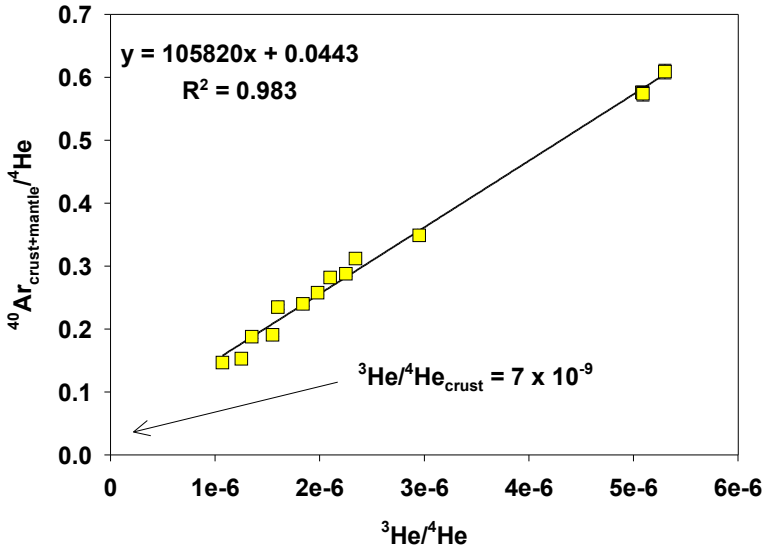
y = 105820x + 0.0443
R2 = 0.983
3He/4Hecrust = 7 x 10-9
40Arcrust+mantle/4He
3He/4He
0.7
0.6
0.5
0.4
0.3
0.2
0.1
0.0
0
1e-6
2e-6
3e-6
4e-6
5e-6
6e-6

Fig. 6. (a) top. (b) bottom. Resolving crust and mantle end members using simple mixing. Elemental Ne/He **(a)** and Ar/He **(b)** ratios plotted against $^{3}He/^{4}He$ for samples from Bravo Dome exhibit simple mantle-crust two component mixing lines. Extrapolation to the crustal $^{3}He/^{4}He$ end member value allows the crustal input ratios to be determined.

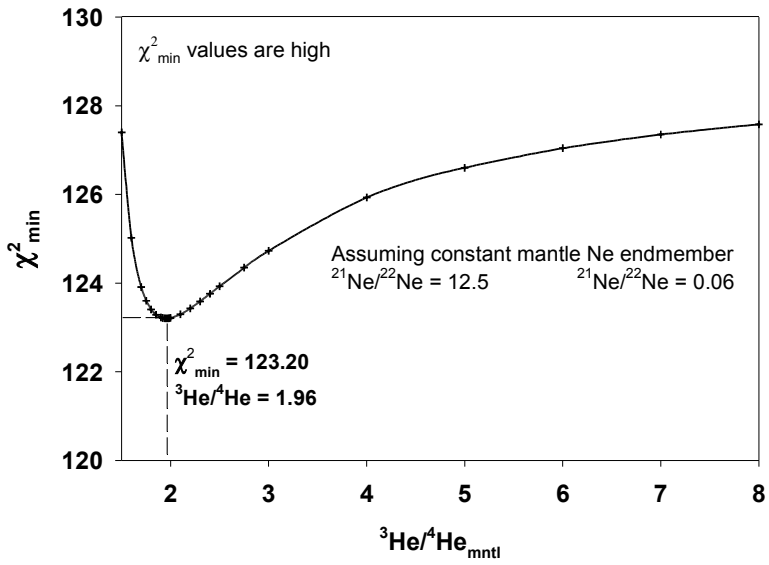

Fig. 7. X^2 minimization on the variance of resolved $^4He/^{21}Ne_{crust}$ values as a function of $^3He/^4He_{mantle}$ end member. The variance in the $^4He/^{21}Ne_{crust}$ values minimizes to a $^3He/^4He_{mantle}$ ratio of 1.96 Ra. However the X^2_{min} value of 123.20 is too high to provide a statistically significant resolution of the $^3He/^4He_{mantle}$ ratio within the field.

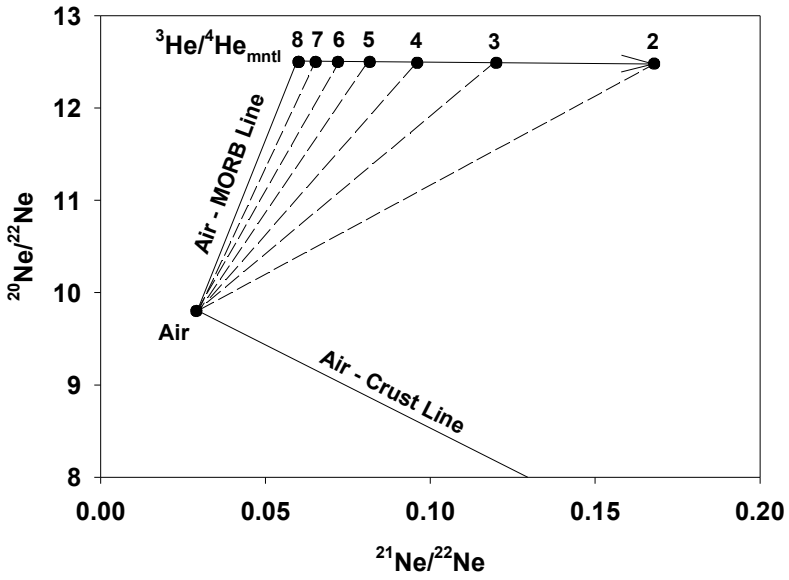

Fig. 8. Plot of the $^{20}Ne/^{22}Ne$ against $^{21}Ne/^{22}Ne$ showing the effect of mantle radiogenic addition on the $^{21}Ne/^{22}Ne_{mantle}$ ratio correlated with a reduction of the $^{3}He/^{4}He_{mantle}$ ratio from 8 to 2 Ra.

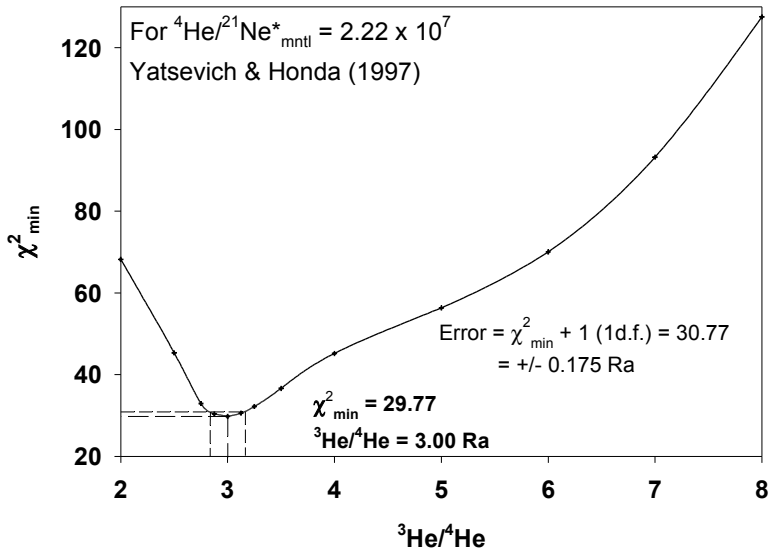

Fig. 9. X^2 minimization on the variance of resolved $^4He/^{21}Ne_{crust}$ values as a function of $^3He/^4He_{mantle}$ end member and corresponding increase in $^{21}Ne/^{22}Ne$ using a $^4He/^{21}Ne^*_{mantle}$ ratio of 2.22 x 10^7. The variance of $^4He/^{21}Ne_{crust}$ minimizes to a $^3He/^4He_{mantle}$ ratio of 3.00 Ra. For 1 degree of freedom the 68.3% confidence limit is determined by the X^2_{min} value + 1. This gives a range of $^3He/^4He_{mantle}$ of 3.00 ± 0.18 Ra corresponding to a resolved $^4He/^{21}Ne_{crust}$ value of 3.08 ± 0.32.

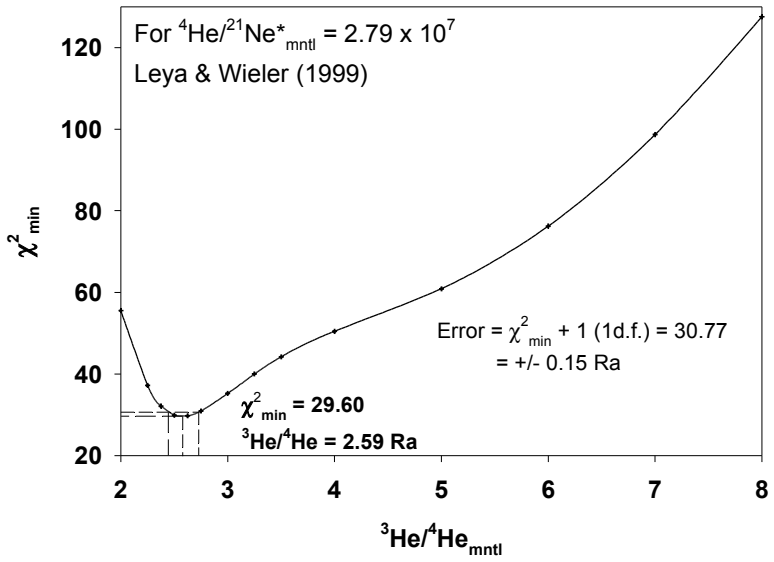

Fig. 10. χ^2 minimization on the variance of resolved $^4He/^{21}Ne_{crust}$ values as a function of $^3He/^4He_{mantle}$ end member and corresponding increase in $^{21}Ne/^{22}Ne$ using a $^4He/^{21}Ne^*_{mantle}$ ratio of 2.79 x 10^7. The variance of $^4He/^{21}Ne_{crust}$ minimizes to a $^3He/^4He_{mantle}$ ratio of 2.59 Ra ± 0.15 Ra corresponding to a resolved $^4He/^{21}Ne_{crust}$ value of 2.90 ± 0.30.

Fig. 11. χ^2 minimization on the variance of resolved $^{21}Ne/^{40}Ar_{crust}$ values as a function of $^{4}He/^{40}Ar_{mantle}$ end member. The variance of $^{21}Ne/^{40}Ar_{crust}$ minimizes to a $^{4}He/^{40}Ar_{mantle}$ ratio of 1.00, +0.20, -0.11 for a $^{3}He/^{4}He_{mantle}$ ratio of 2.59 Ra, and to a ratio of 0.85, +0.18, -0.08 for a $^{3}He/^{4}He_{mantle}$ of 3.00 Ra.

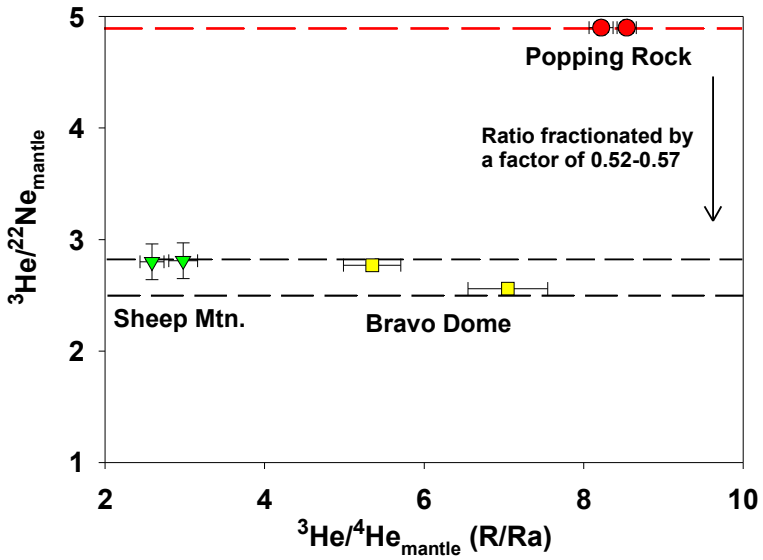

Fig. 12. Plot of the resolved elemental $^3He/^{22}Ne_{mantle}$ against the corresponding mantle $^3He/^4He_{mantle}$ for the two gas fields. Both Bravo Dome and Sheep Mountain exhibit a similar reduction (factor of 0.52 - 0.57) in $^3He/^{22}Ne_{mantle}$ ratios compared to the values observed in MORB.

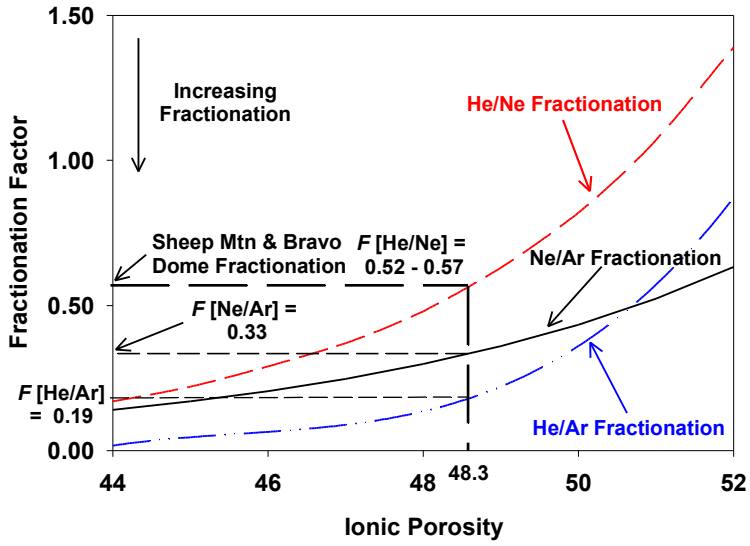

Fig. 13. Plot of the fractionation factor against % melt ionic porosity for He/Ne, Ne/Ar and He/Ar. Maximum fractionation occurs in the gas phase as the gas/melt volume approaches zero. Data from Carroll and Draper (1994) are used. For He/Ne a maximum melt ionic porosity of 48.4% is required to account for the fractionation observed in both Sheep Mountain and Bravo Dome.

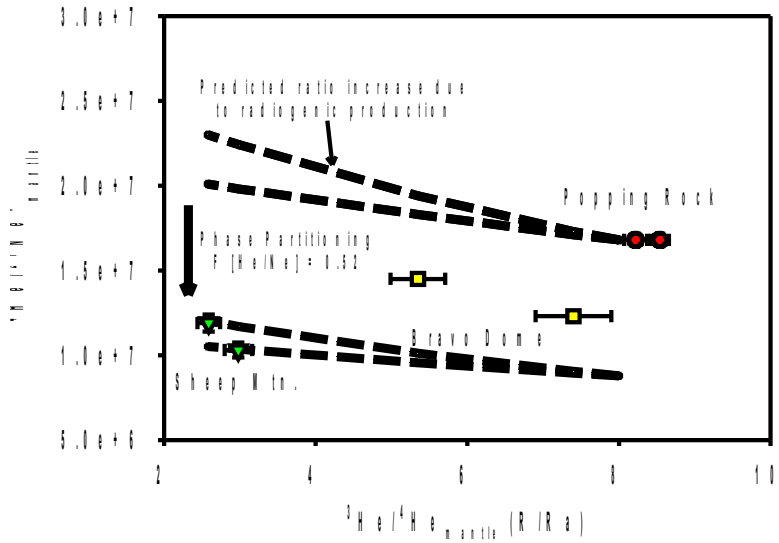

Fig. 14. Plot of the resolved radiogenic $^4He/^{21}Ne^*_{mantle}$ against the corresponding mantle $^3He/^4He_{mantle}$ for Bravo Dome and Sheep Mountain. Also shown is the predicted ratio increase which would result from radiogenic production of ^4He and ^{21}Ne in the mantle, and how these ratios would be reduced by the same degree of phase partitioning as the maximum observed in the $^3He/^{22}Ne_{mantle}$ ratios (F = 0.52). Significantly, the range of values resolved in both fields can be accounted for by a combination of these two processes.

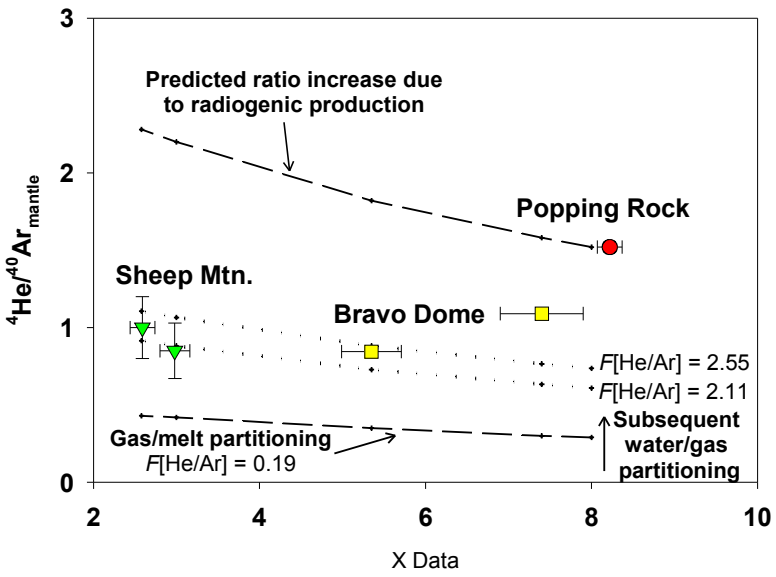

Fig. 15. Plot of the resolved $^{3}He/^{4}He_{mantle}$ ratio against the corresponding $^{4}He/^{40}Ar_{mantle}$ range. The $^{3}He/^{4}He_{mantle}$ and $^{4}He/^{40}Ar_{mantle}$ values from both fields can be explained by radiogenic ingrowth in the mantle source combined with gas/melt phase partitioning and subsequent water/gas partitioning.

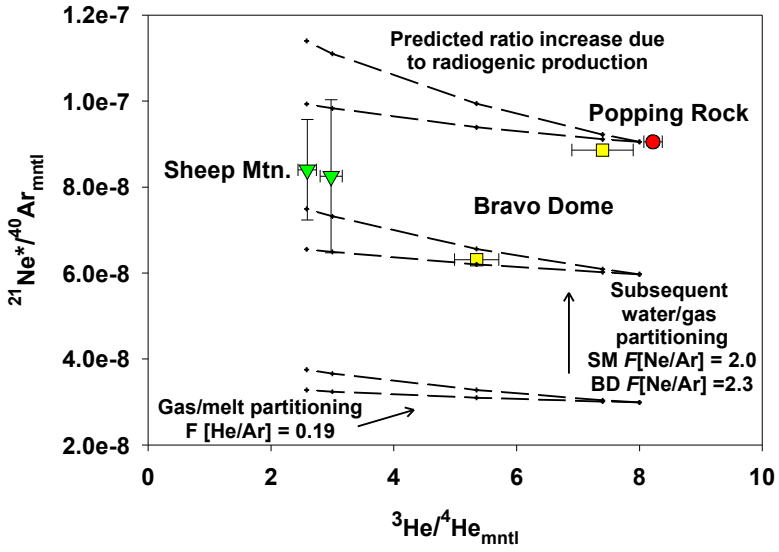

Fig. 16. Plot of the resolved $^{3}He/^{4}He_{mantle}$ against $^{21}Ne/^{40}Ar_{mantle}$. The $^{3}He/^{4}He_{mantle}$ and $^{21}Ne^{40}Ar_{mantle}$ values from Sheep Mountain and the lower value from Bravo Dome can be explained by a similar radiogenic ingrowth and phase partitioning model as outlined above. However, the upper Bravo Dome value which is not significantly lower than MORB cannot be accounted for.

Table 1. Sample location and noble gas isotope ratios

1σ errors quoted in brackets. $^{3}He/^{4}He$ are relative to the atmospheric ratio ($R/Ra = 1.39 \times 10^{-6}$)

Field & Well	Location Sec/Twp/Rge Lat/Long	$^{3}He/^{4}He$	$^{20}Ne/^{22}Ne$	$^{21}Ne/^{22}Ne$	$^{40}Ar/^{36}Ar$	$^{130}Xe/^{136}Xe$
Sheep Mtn						
8-2-P	2/9-28S/70W	0.981 (0.010)	10.14 (0.06)	0.0410 (0.0002)	13839 (41)	0.422 (0.002)
2-10-O	15/9-27S/70W	0.984 (0.012)	10.08 (0.05)	0.0377 (0.0002)	10744 (39)	0.421 (0.002)
9-26	26/9-27S/70W	0.934 (0.014)	10.19 (0.08)	0.0461 (0.0003)	16486 (67)	0.417 (0.001)
2-9-H	9/9-27S/70W	0.945 (0.019)	10.11 (0.06)	0.0312 (0.0003)	4378 (21)	0.444 (0.004)
3-15-B	15/9-27S/70W	0.937 (0.016)	10.11 (0.06)	0.0375 (0.0003)	8745 (19)	0.430 (0.003)
4-13		0.942 (0.018)	10.20 (0.06)	0.0405 (0.0003)	17292 (92)	0.416 (0.002)
4-26-E	26/9-27S/70W	1.024 (0.018)	10.29 (0.11)	0.0614 (0.0003)	21203 (46)	0.412 (0.002)
3-23-D	22/9-27S/70W	0.988 (0.014)	10.15 (0.04)	0.0535 (0.0003)	16956 (42)	0.418 (0.003)
7-35-L	2/9-28S/70W	0.916 (0.014)	10.23 (0.03)	0.0511 (0.0003)	17590 (33)	0.414 (0.002)
2-35-C	26/9-27S/70W	0.963 (0.019)	10.29 (0.08)	0.0528 (0.0003)	16566 (49)	0.426 (0.002)
1-15-C	15/9-27S/70W	0.967 (0.016)	9.94 (0.06)	0.0311 (0.0003)	5194 (30)	NM
3-4-O	9/9-27S/70W	0.937 (0.014)	9.93 (0.09)	0.0342 (0.0003)	4538 (10)	0.416 (0.003)
4-14-M	22/9-27S/70W	0.892 (0.015)	9.97 (0.06)	0.0404 (0.0003)	17895 (173)	0.440 (0.001)
5-15-O	22/9-27S/70W	1.056 (0.015)	9.89 (0.06)	0.0319 (0.0003)	8720 (25)	0.422 (0.002)
4-4-P	9/9-27S/70W	0.970 (0.014)	10.15 (0.08)	0.0440 (0.0003)	16010 (36)	0.417 (0.002)
5-9-A	9/9-27S/70W	1.006 (0.018)	10.15 (0.03)	0.0428 (0.0003)	17813 (38)	0.419 (0.001)
1-1-J	2/9-28S/70W	0.908 (0.016)	9.84 (0.03)	0.0407 (0.0003)	12037 (22)	NM
1-22-H	22/9-28S/70W	0.981 (0.017)	10.03 (0.02)	0.0401 (0.0003)	10864 (69)	NM
Bravo Dome						
BD01	23/19N/34E	1.670 (0.008)	10.66 (0.03)	0.0562 (0.0003)	10700 (314)	0.432 (0.001)
BD02	32/21N/35E	0.764 (0.004)	9.96 (0.03)	0.0501 (0.0003)	4654 (41)	NM
BD03	36/22N/34E	0.896(0.004)	10.01 (0.01)	0.0515 (0.0001)	5342 (71)	0.419 (0.001)
BD04	8/20N/34E	1.611 (0.008)	10.59 (0.04)	0.0541 (0.0004)	9886 (185)	0.430 (0.001)
BD05	34/20N/35E	0.965 (0.005)	9.93 (0.01)	0.0526 (0.0002)	5408 (38)	NM
BD06	26/22N/32E	1.503 (0.008)	10.49 (0.04)	0.0561 (0.0004)	9197 (161)	0.423 (0.002)
BD07	3/19N/33E	2.104 (0.011)	11.20 (0.05)	0.0542 (0.0004)	10923 (308)	NM
BD08	9/18N/33E	1.143 (0.006)	10.21 (0.03)	0.0578 (0.0004)	6643 (65)	NM
BD09	17/21N/33E	1.724 (0.009)	10.74 (0.05)	0.0578 (0.0005)	NM	NM
BD10	7/22N/34E	1.104 (0.006)	10.20 (0.02)	0.0537 (0.0003)	6719 (81)	NM
BD11	25/19N/30E	3.784 (0.019)	11.88 (0.05)	0.0565 (0.0004)	21453 (1274)	NM
BD12	27/19N/30E	3.627 (0.018)	NM	NM	20888 (1017)	0.425 (0.002)
BD13	22/18N/35E	1.318 (0.007)	10.25 (0.05)	0.0579 (0.0005)	7714 (220)	NM
BD14	16/18N/34E	1.413 (0.007)	10.54 (0.12)	0.0583 (0.0002)	8490 (523)	NM
BD12b	27/19N/30E	3.634 (0.018)	11.60 (0.06)	0.0537 (0.0002)	22492 (2474)	NM

NM = Not Measured.

Table 2. Noble gas concentrations (cm^3STP/cm^3)

Field & Well	^{4}He (x 10^{-4})	^{20}Ne (x 10^{-8})	^{40}Ar (x 10^{-4})	^{84}Kr (x 10^{-10})	^{130}Xe (x 10^{-12})
Sheep Mtn					
8-2-P	3.13 (0.03)	1.47 (0.02)	1.67 (0.01)	2.96 (0.25)	4.76 (0.08)
2-10-O	2.96 (0.03)	3.04 (0.03)	1.62 (0.01)	3.10 (0.30)	4.65 (0.08)
9-26	2.95 (0.03)	0.613 (0.009)	1.57 (0.02)	4.19 (1.91)	4.11 (0.07)
2-9-H	3.07 (0.03)	9.77 (0.10)	1.39 (0.01)	5.54 (1.14)	8.93 (0.15)
3-15-B	2.90 (0.03)	1.54 (0.02)	1.60 (0.02)	9.85 (1.84)	6.50 (0.11)
4-13	3.47 (0.04)	1.11 (0.02)	2.08 (0.02)	4.58 (1.96)	5.63 (0.10)
4-26-E	3.15 (0.03)	0.442 (0.004)	1.73 (0.01)	7.16 (4.03)	4.47 (0.08)
3-23-D	3.17 (0.03)	0.579 (0.009)	1.84 (0.02)	8.48 (2.62)	3.27 (0.06)
7-35-L	3.06 (0.03)	0.749 (0.012)	1.56 (0.01)	5.36 (0.53)	5.22 (0.09)
2-35-C	2.87 (0.03)	0.573 (0.008)	1.57 (0.01)	2.71 (0.48)	4.79 (0.08)
1-15-C	2.71 (0.03)	6.77 (0.10)	1.55 (0.02)	5.00 (2.09)	NM
3-4-O	2.99 (0.03)	2.64 (0.03)	1.57 (0.01)	8.61 (0.54)	4.89 (0.09)
4-14-M	3.00 (0.03)	1.11 (0.01)	1.63 (0.02)	2.09 (0.52)	1.06 (0.18)
5-15-O	2.92 (0.03)	4.33 (0.05)	1.51 (0.01)	3.69 (0.34)	5.44 (0.09)
4-4-P	2.52 (0.02)	1.31 (0.02)	1.60 (0.02)	2.73 (0.50)	5.52 (0.10)
5-9-A	2.94 (0.03)	1.28 (0.02)	2.06 (0.01)	3.05 (0.50)	3.15 (0.06)
1-1-J	2.16 (0.02)	0.878 (0.012)	1.66 (0.01)	5.29 (0.09)	NM
1-22-H	3.22 (0.03)	0.937 (0.013)	1.55 (0.01)	5.72 (0.11)	NM
Bravo Dome					
BD01	0.944 (0.012)	0.169 (0.002)	0.303 (0.003)	1.01 (0.02)	NM
BD02	4.15 (0.05)	0.700 (0.007)	0.652 (0.006)	5.04 (0.14)	9.83 (0.40)
BD03	3.31 (0.04)	0.521 (0.005)	0.536 (0.005)	3.24 (0.08)	NM
BD04	9.61 (0.02)	0.181 (0.002)	0.286 (0.003)	1.03 (0.03)	2.09 (0.09)
BD05	2.70 (0.04)	0.446 (0.004)	0.538 (0.005)	3.33 (0.08)	6.15 (0.26)
BD06	1.20 (0.02)	0.202 (0.002)	0.350 (0.003)	1.35 (0.04)	NM
BD07	0.781 (0.010)	0.180 (0.002)	0.280 (0.003)	0.900 (0.036)	1.96 (0.10)
BD08	1.61 (0.02)	0.264 (0.003)	0.396 (0.004)	2.00 (0.05)	NM
BD09	0.981 (0.012)	0.180 (0.002)	NM	NM	NM
BD10	1.99 (0.03)	0.308 (0.003)	0.396 (0.003)	2.02 (0.05)	NM
BD11	0.391 (0.005)	0.103 (0.001)	0.241 (0.004)	0.455 (0.019)	9.94 (0.09)
BD12	0.415 (0.006)	NM	0.242 (0.003)	0.467 (0.024)	NM
BD13	1.53 (0.02)	0.240 (0.003)	0.382 (0.004)	1.92 (0.05)	3.18 (0.06)
BD14	1.15 (0.02)	0.179 (0.004)	0.307 (0.003)	1.23 (0.04)	NM
BD12b	0.413 (0.006)	0.120 (0.002)	0.240 (0.004)	0.490 (0.024)	NM

Table 3. Resolved mantle elemental and isotopic ratios.

Source	$^{3}He/^{4}He_{mantle}$ (Ra)	$^{4}He/^{21}Ne^{*}_{mantle}$ ($x10^{7}$)	$^{3}He/^{22}Ne_{mantle}$	$^{4}He/^{40}Ar_{mantle}$	$^{21}Ne/^{40}Ar_{mantle}$ ($x10^{-8}$)
Popping Rock (Moreira et al., 1998; *Burnard et al., 1997)	8.22 ± 0.15* 8.54 ± 0.12	1.68	4.90	1.52	6.31 9.05
Bravo Dome (Ballentine et al., 2005; 'Holland and Ballentine, 2006)	5.35 ± 0.36 7.40 ± 0.50'	1.45 1.23'	2.77 2.56'	0.844 1.09'	5.82 8.86'
Sheep Mountain	2.59 ± 0.15 2.98 ± 0.18	1.19 ± 0.07 1.03 ± 0.06	2.80 ± 0.16 2.81 ± 0.16	1.00 +0.20, -0.11 0.85 +0.18, -0.08	8.40 ± 1.17 8.25 ± 1.78

$^{21}Ne^{*}$ indicates ^{21}Ne corrected for solar contribution [53]